Materials and Design 85 (2015) 309–317

Contents lists available at ScienceDirect

Materials and Design

journal homepage: www.elsevier.com/locate/jmad

Effect of humidity on porosity, microstructure, and fatigue strength of A7N01S-T5 aluminum alloy welded joints in high-speed trains

G. Gou [a], M. Zhang [a], H. Chen [a], J. Chen [a,b], P. Li [c], Y.P. Yang [d,*]

[a] School of Materials Science and Engineering, Southwest Jiaotong University, Chengdu 610031, China
[b] Chengdu Technician College, Chengdu 611731, China
[c] CSR Qingdao Sifang Co. Ltd, Qingdao 266000, China
[d] EWI, Columbus, OH 43221, USA

ARTICLE INFO

Article history:
Received 27 March 2015
Received in revised form 29 June 2015
Accepted 30 June 2015
Available online 5 July 2015

Keywords:
Aluminum alloy
Welding
Humidity
Porosity
Fatigue
High-speed train

ABSTRACT

Humidity is a key factor affecting the quality of welded joints for high-speed trains. Welded joints made of A7N01S-T5 aluminum alloy were fabricated under five relative environmental humidity conditions: 50%, 60%, 70%, 80%, and 90%. The microstructures of the welded joints were examined using an optical microscope and porosity quantities were calculated from macrographs using image analysis software. The fatigue strength of the welded joints was measured with high-cycle fatigue testing. It was determined that the microstructures and grain sizes in the weld zone and heat-affected zone (HAZ) were similar under different humidity conditions; however, porosity distribution varied significantly. Porosity quantity increased as humidity increased. The weld joint made under the 90% humidity condition had the highest quantity of porosity, while the weld joint made under the 70% humidity condition had the maximum diameter and area of porosity. The weld joint made under the 70% humidity condition also had the lowest fatigue strength. Fracture morphology of fatigue samples showed that the weld joint made under the 70% humidity condition had brittle fracture, while others showed ductile fracture. Therefore, 70% humidity was determined to be the critical humidity level for welding joints in high humidity environment.

1. Introduction

A7N01S-T5 is an Al–Zn–Mg alloy with high strength, good extrusion, and good welding properties that can be extruded into thin-walled sections with complex shapes. It has been selected to make the welded components of high-speed trains, such as under-frames, corbels, and other key important parts subjected to static and dynamic loading. Weld-joint failures were found in the welded components during service. Weld defects contributed significantly to the failures [1–3].

Porosity is one of the main defects produced in gas metal arc welding (GMAW) of aluminum–alloy structures during fabrication of high-speed trains. Hydrogen (H) is the main contributor to porosity during welding [4–10]. When the humidity is higher, the high temperature surrounding the welding arc promotes decomposition of water (H_2O) in the air to H ions. The amount of dissolution of H ions in the weld pool is proportional to the H-ion concentration. The solubility of H ions decreases as the temperature of the weld pool decreases during cooling. Thus, the H ions will escape from the weld pool during cooling by forming bubbles and floating to the surface. Bubbles that do not escape the weld pool become porosity.

Research results [11–17] indicate that humidity plays an important role in the formation of hydrogen-induced porosity in weld joints and conclude that porosity results a reduction in strength. The content of diffusible H ions increased with an increase in water-vapor pressure in the air. Therefore, the sensitivity of porosity formation increased with an increase in humidity. When the humidity was higher, the weld microstructure grains became coarser, and porosity size increased in the fusion zone and heat-affected zone (HAZ).

There is a little research to quantify the effect of humidity in the air on porosity, microstructure, and fatigue strength in a welded joint. As a result, a critical level of humidity in which welding should not be conducted has not been established. Zhou et al. [18] studied the effects of ambient temperature and humidity on porosity formation in weld metal. A simulated gas chamber was designed and made for welding tests. Experiments were done under various temperature and humidity conditions; however, Zhou et al. did not study the effect of porosity on the microstructure and mechanical properties of weld joints. Shore and McCauley [19] studied the effect of porosity on high strength 7039 aluminum and concluded that porosity reduced both weld metal ductility and fatigue life. Rudy and Rupert [20] studied the effect of porosity on the mechanical properties of aluminum welds and found that increasing area fractions of porosity in a weld cross section would reduce strength. They also found that fine porosity also reduced the joint strength as much as a large porosity did, if present in sufficient

* Corresponding author.
E-mail address: yyang@ewi.org (Y.P. Yang).

http://dx.doi.org/10.1016/j.matdes.2015.06.177
0264-1275/

Table 1
Chemical composition of A7N01S-T5 matrix and ER5356 filler wire.

Materials	Chemical composition (wt.%)									
	Zn	Mg	Cu	Mn	Cr	Ti	Zr	Si	Fe	Al
A7N01	4.190	1.340	0.011	0.317	0.233	0.043	0.122	0.046	0.100	Bal.
ER5356	≤0.10	4.5–5.5	≤0.10	0.05–0.20	0.05–0.20	0.06–0.2	–	≤0.25	≤0.10	Bal.

quantity. The components of high-speed trains have been welded under many different environments all over the world. Every place has its own temperature and humidity. Therefore, it is important to understand the effect of humidity on porosity, microstructures and fatigue properties of welded joints made of A7N01S-T5 aluminum alloy.

2. Materials and experimental work

2.1. Materials

Experimental base material consisted of 8-mm think A7N01S sheets that had undergone T5 heat treatment (cooled from an elevated-temperature during shaping process and then artificially aged according to ISO 2107:2007). The times and temperatures for aging were 10 h in the first 100 °C and then 10 h for 150 °C. To remove oxides and decrease the possibility of porosity in weld joints, the surface of welded samples was chemically cleaned.

Welded joint samples were made using GMAW with 1.2 mm diameter ER5356 filler wire. The chemical compositions of the A7N01S-T5 base material and ER5356 are listed in Table 1. The mechanical properties of the A7N01S-T5 base material are listed in Table 2.

2.2. Welding process

To adjust the humidity of the welding environment, an environment simulation lab, as shown in Fig. 1, was established to enable the creation of relative humidity conditions of 50%, 60%, 70%, 80%, and 90%. The temperature in the lab was adjustable between −30 °C and 40 °C and the wind velocity was variable between 0 m/s and 4 m/s.

The five levels of relative humidity were selected for two reasons. The first reason is that the porosity sizes were tiny and the quantity was minimal under a 50% relative humidity condition. The second reason is that it is required by the manufacturing standard that the humidity should be equal or below 70%. This paper studied the variation of humidity by + or −20%.

Welding process parameters, as shown in Table 3, were developed by carrying out a large number of welding experiments to achieve defect-free weld joints under normal welding conditions. During welding experiments, 99.999% pure argon was used as the shielding gas for the GMAW torch and paraxial gas nozzle.

2.3. Microstructure examination and porosity quantity measurement

The microstructures of the samples welded under different humidity were examined using a Zeiss AX10 optical microscope. Samples were prepared by cutting the weld joints perpendicular to the welding direction. The polished samples were etched using mixed acid solution (volume ratio: 1%HF, 1.5%HCL, 2.5%HNO_3, and 95%H_2O), with an etching time of 20–30 s.

The cross sections of the welded joints first were examined using a VK1000 stereomicroscope and then the porosity quantity was analyzed with Image-Pro Plus software based on a color-difference analysis method. Fig. 2 shows an example image for developing the test procedure.

2.4. Fatigue test

Fatigue samples were machined from the welded blanks in the direction perpendicular to the welding direction. Weld reinforcements in the fatigue samples were removed to meet the test standard requirement. Fig. 3 shows the dimensions of the fatigue samples. Before fatigue testing, all samples were visually inspected to ensure no macroscopic defects.

Fatigue tests were performed on electromagnetic resonant high-cycle fatigue equipment by applying a tension–compression cyclic load at a zero stress ratio. The test waveform was a sine wave and the test frequency was in the range from 90 Hz to 110 Hz. The maximum number of loading cycles was 1×10^7 was considered the fatigue limit if the samples were not broken. The fracture surfaces of the broken fatigue samples were observed using a scanning electron microscope (SEM) to identify fatigue crack initiation locations as well as the propagation mechanism.

3. Results and discussion

3.1. Microstructures of welded joints

Microstructures and cross-sectional macrographs of weld joints under the different humidity are shown in Fig. 4. The microstructures under different humidity were similar in the weld zone and HAZ. In the weld zone, the uniform equiaxed grains had diameters between 90 μm to 105 μm and the main microstructures were composed of α-Al solid solution and α-Al + β-Al_8Mg_5 eutectic phases. In the heat-affected zones, inhomogeneous microstructures and coarse grains induced by overheating were observed. The grains were round shapes and the microstructures were columnar crystals arranged along the direction of heat transferring from the fusion lines. The grains sizes in the HAZ were much larger than the weld zone for all humidity conditions. This resulted from the non-spontaneous nucleation along the fusion line in the HAZ that was heated to semi-molten state during welding.

By comparing the cross-sectional morphologies under different humidity conditions, it was determined, that that porosity was dispersedly distributed and the quantity increased with increased humidity. Under the 50% humidity condition, the porosity sizes were tiny and the quantity was minimal. Under the 60% humidity condition, the size and quantity of porosity increased slightly. Under the 70% humidity condition, the size and quantity of porosity increased sharply. Larger pores were dispersedly distributed along the fusion line of weld. Under the 80% humidity condition, the porosity size decreased while the quantity increased. Under the 90% humidity condition, the porosity sizes further decreased, the quantity further increased, and the distribution was more uniform than under other humidity conditions.

Table 2
Mechanical properties of A7N01S-T5.

Materials	Hardness (HV)	Tensile strength(MPa)	Yield strength(MPa)	Elongation (%)	Impact toughness (J/cm^2)	Fatigue strength (MPa)
A7N01S-T5	107	393	327	15.5	24	174.5

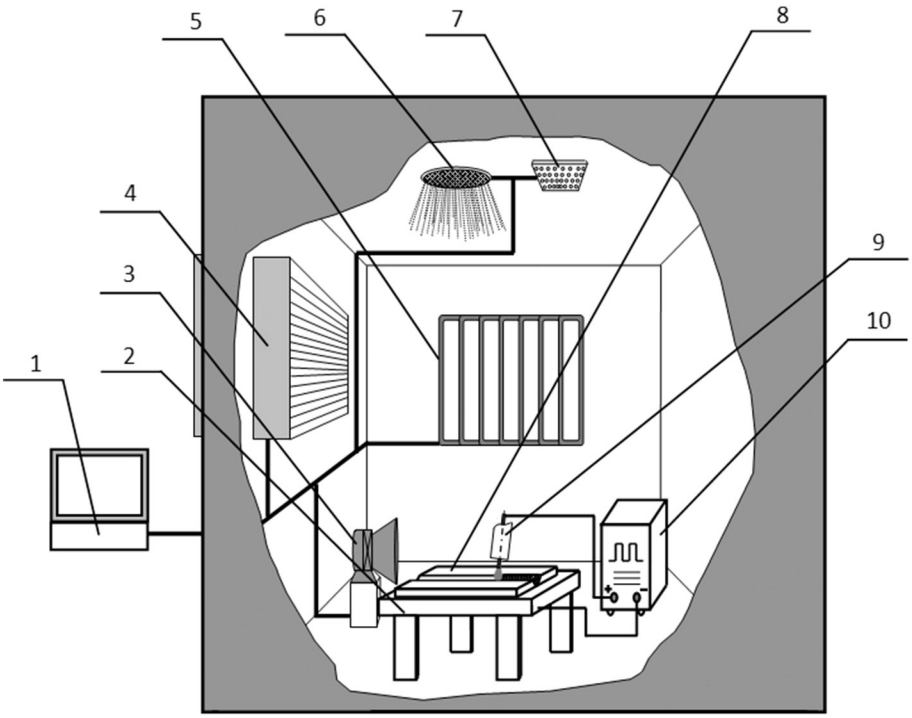

Fig. 1. Design of welding-environment simulation lab. 1—welding expert database and control system; 2—welding table; 3—wind flow speed control device; 4—device for reducing temperature; 5—device for increasing temperature; 6—humidification intelligent control device; 7—dehumidification intelligent control device; 8—weldment; 9—welding torch; 10—welding machine.

Table 4 and Fig. 5 show the porosity statistics and trends for relative humidities from 50% to 90%. The results showed that the porosity under the 70% humidity condition had the maximum mean size, maximum diameter, maximum area, maximum total area, maximum cross-sectional total area, and maximum possession rate. The possession rate is the percentage of total porosity area over the weld area. The porosities under the 90% humidity condition had the maximum quantity. According to ISO 10042:2006, the porosity quantity and quality under the 50% humidity was at "A" grade (considered free of porosity defects). The porosity quantity and quality under the humidity 60%, 80%, and 90% reached to "B" grade (not believed to decrease the static strength of welded joints). The porosity quantity and quality under the 70% humidity reached to "C" grade (joints welded under this humidity condition could not be used as engineering structures). Therefore, the 70% humidity is a critical point that could affect the mechanical properties of welded joints.

3.2. Fatigue property

3.2.1. P–S–N curves for the welded samples

The following equations were used to process the measured data in the fatigue testing to get the P–S–N curves according ISO 12107:2012. P stands for the failure probability, N is the number of cycles, and S is the stress amplitude.

$$x = \hat{b} - \hat{a}y \tag{1}$$

$$\hat{a} = -\frac{\sum_{i=1}^{n}(x_i-\overline{x})(y_i-\overline{y})}{\sum_{i=1}^{n}(y_i-\overline{y})^2} \tag{2}$$

$$\hat{b} = \overline{x} + \hat{a}\overline{y} \tag{3}$$

$$\hat{\sigma}_x = \sqrt{\frac{\sum_{i=1}^{n}\left[x_i-\left(\hat{b}-\hat{a}y_i\right)\right]^2}{n-2}} \tag{4}$$

$$\hat{\sigma}_y = \frac{\hat{\sigma}_x}{\hat{a}} \tag{5}$$

$$\hat{x}_{(P,1-\alpha,v)} = \hat{b} - \hat{a}y - k_{(P,1-\alpha,v)}\hat{\sigma}_x \sqrt{1+\frac{1}{n}+\frac{(y-\overline{y})^2}{\sum_{i=1}^{n}(y_i-\overline{y})^2}} \tag{6}$$

Table 3
Welding process parameters for A7N01S-T5.

Materials	Thickness (mm)	Weld	Peak current (A)	Voltage (V)	Welding speed (mm/min)	Environment temperature (°C)	Environment humidity (%)
A7N01S-T5	8	1	170–189	20.3–22.7	600–656	24–26 °C	50–90%
		2	174–195	21.4–22.9	636–656		
		3	176–191	22.1–23.2	500–525		

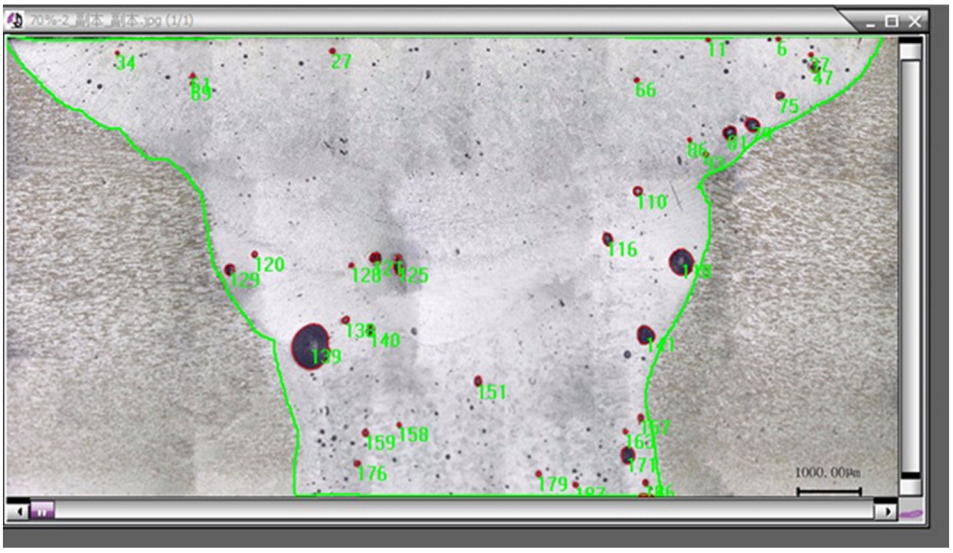

Fig. 2. Image of porosity measurement in cross sections.

$$\hat{\mu}_y = \frac{\sum_{i=2}^{n+1} S_i}{n} \tag{7}$$

$$\hat{y}_{(P,1-\alpha)} = \hat{\mu}_y - k_{(P,1-\alpha,\nu)}\hat{\sigma}_y \tag{8}$$

where $x = \lg N$ and $y = S$. x_i and y_i are the measured values from fatigue testing. $\bar{x}$ and $\bar{y}$ are the average value of x_i and y_i, respectively. n is the data points and $\upsilon = (n-2)$ is degree of freedom (DOF). $\hat{\sigma}_x$ is the standard deviation of logarithmic fatigue life for the total samples and $\hat{\sigma}_y$ is the standard deviation of fatigue strength for the total samples. $(1-\alpha)$ is the confidence probability, k is the unilateral error of normal, $\hat{\mu}_y$ is the mean fatigue strength under the failure probability 50%, and $\hat{y}_{(P,1-\alpha)}$ is the mean fatigue strength under the confidence probability $(1-\alpha)$.

Fig. 6 shows the P–S–N curves of welded joints under different humidity conditions. Each figure contains measured data and two lines. The upper line is for a 50% failure probability (50% confidence) and the lower line is for a 90% failure probability (10% confidence). Note that the number of cycles was plotted with logarithm values. For a stress of 110 MPa, the logarithmic number of cycles for 50% confidence under the humidity 50%, 60%, 70%, 80%, and 90% was about 6.9, 6.7, 5.2, 5.9, and 6.0, respectively. Therefore, the fatigue life was reduced with the increase of humidity in general. The weld samples welded under the 70% humidity had the lowest fatigue life.

Fig. 7a and b show the mean fatigue strength under different humidity conditions for the failure probability 50% and 10%, respectively, which provide the change trend of the mean fatigue strength with the increase of humidity. The mean fatigue strength decreases from 50% humidity to 70% humidity and then increases to 90% humidity. There is a large drop of the mean fatigue strength under the humidity 70%.

In summary, the fatigue samples welded under the 50% humidity showed the best fatigue performance with fatigue strength 103.75 MPa for the number of cycles 10^7, while the fatigue samples welded under the 70% humidity showed the lowest fatigue performance with fatigue strength 68.67 MPa for the same number of cycles. The mean fatigue strength for the 70% humidity was only 66% of that for the 50% humidity. For the 10% failure probability, the mean fatigue strength under the 70% humidity was even lower, only 58% of that for the 50% humidity. Because the weld reinforcement was removed for all fatigue samples, it can be assumed that all of these samples had the same surface condition. Therefore, the fatigue strength of the welded joint is largely determined by porosity.

3.2.2. Fracture mechanism study

Fig. 8 shows the fracture morphologies of a broken fatigue sample under the 50% humidity condition. The fatigue cracks originated from the accumulated porosity zone near the left surface, propagated throughout internally, and finally fractured, as shown in Fig. 8a.

Fig. 9 shows the fracture morphologies of a broken fatigue sample under the 60% humidity condition. The macrofatigue stairs show the fatigue crack initialization (see Fig. 9a). The distributed microporosities whose diameters are less than 50 μm may induce stress concentration. There existed striations looming and caves that were introduced by the broken off the impurities, as shown in Fig.9b. These caves may promote crack propagation.

Fig. 10 shows the fracture morphologies of a broken fatigue sample under the 70% humidity condition. The crack source zone showed an arc shape that manifested the crack initiation at a point defect, as

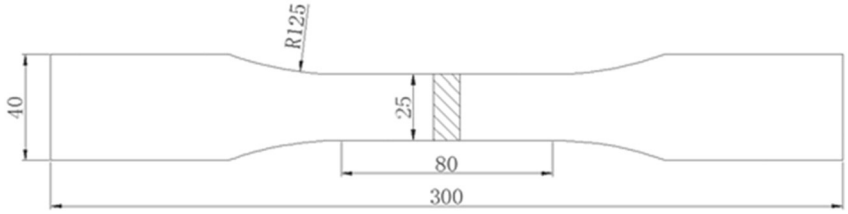

Fig. 3. Dimension of fatigue test samples (all dimensions in mm).

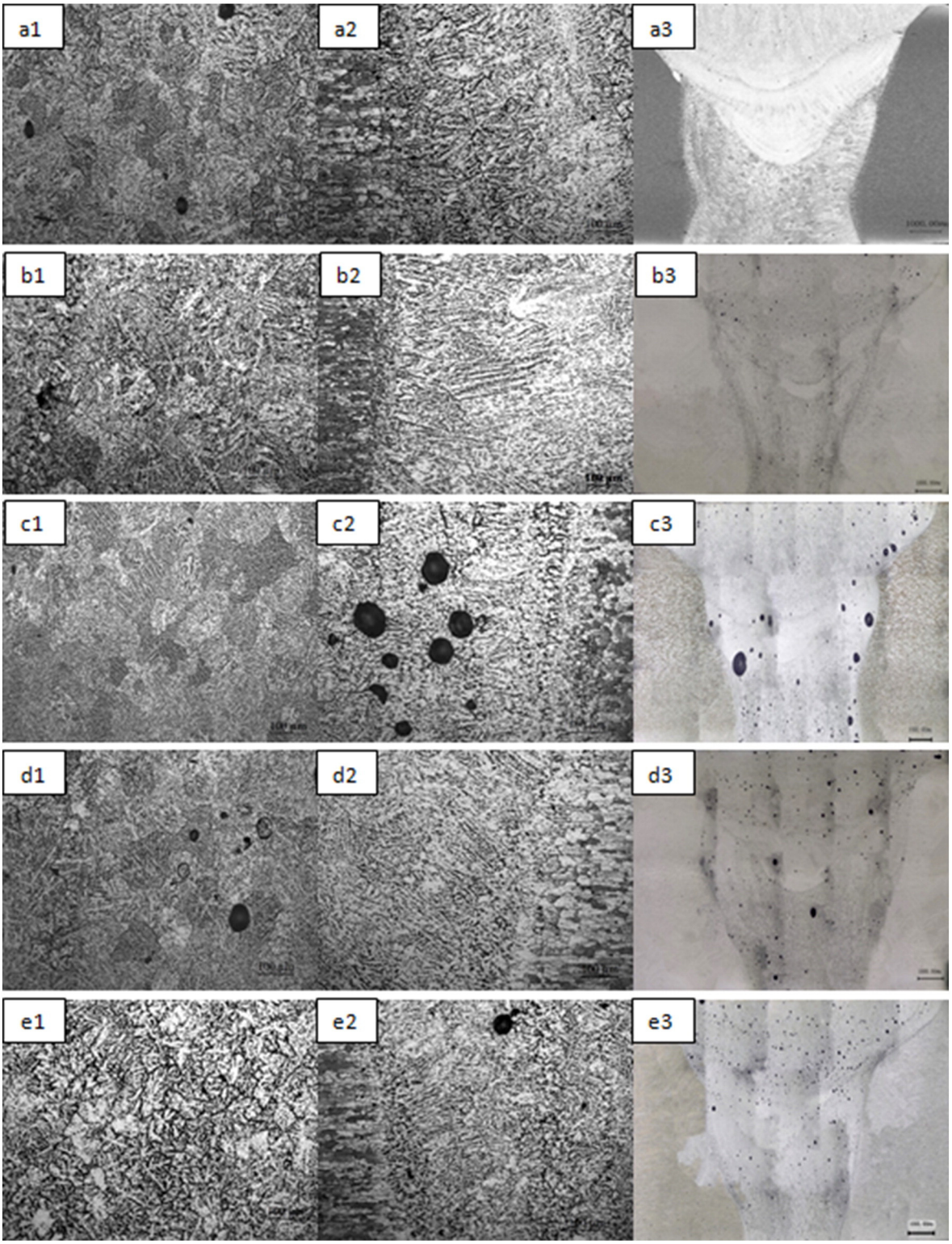

Fig. 4. Microstructures and macrographs of weld under different humidity. (a1) Weld zone under 50% humidity; (a2) fusion line under 50% humidity; (a3) Macrograph under 50% humidity; (b1) Weld zone under 60% humidity; (b2) fusion line under 60% humidity; (b3) Macrograph under 60% humidity; (c1) Weld zone under 70% humidity; (c2) fusion line under 70% humidity; (c3) Macrograph under 70% humidity; (d1) Weld zone under 80% humidity; (d2) fusion line under 80% humidity; (d3) Macrograph under 80% humidity; (e1) Weld zone under 90% humidity; (e2) fusion line under 90% humidity; (e3) Macrograph under 90% humidity.

shown in Fig.10a. A large pore was observed whose diameter was about 700 μm onto the surface. There existed small pores with diameters from 30 μm to 100 μm. The large pore may lead to stress concentration along with the crack. The small pores surrounding the large pore provided the path for crack propagation and reduced fatigue life, as shown in Fig.10b. The fatigue fracture mechanism appears as a brittle fracture.

Fig. 11 shows the fracture microstructures of a fatigue sample under the 80% humidity condition. A large pore with a diameter about 500 μm

Table 4
Porosity content under different humidity.

Humidity (%)	Mean size (mm)	Maximum diameter (mm)	Maximum area (mm^2)	Total area (mm^2)	Sectional total area (mm^2)
50	0.00005	0.06	0.0017	0.002	58.43
60	0.0012	0.11	0.0078	0.14	48.88
70	0.0050	0.72	0.3344	0.96	58.60
80	0.0018	0.29	0.0484	0.35	55.79
90	0.0004	0.16	0.0188	0.21	46.38

appeared near the surface, as shown in Fig. 11a. Stress concentration could occur at the large pore and induce cracking under loading. Small pores with diameters from 30 μm to 100 μm were found on the fracture surface. The cracks propagated and formed the fatigue striations, as shown in Fig.11b; however, the direction of propagation was similar to that observed in Figs. 8b, 9b, and 10b.

Fig. 12 shows the fracture morphologies of a broken fatigue sample for the 90% humidity condition. The fracture zone was in the weld zone and the pores are uniformly and densely distributed on the fracture surface. The largest-diameter of pore was approximately 150 μm, as shown in Fig. 12a. Crack was initiated from the large pore and then propagated to form the fatigue striations, as shown in Fig.12b. However, the direction of propagation was similar to that observed in Figs. 8b, 9b, 10b, and 11b. The pores led to the propagation of the crack until the fracture occurred.

The above experimental results showed that the morphologies were similar under the different humidity but the fracture mechanism of the 70% humidity condition was different from the other humidity conditions. The large pores significantly affected the properties of the welded joints.

Water vapor does not decompose under the temperature 2000 K and decomposes to H_2 and O_2 when the temperature increases from 2000 K to 4800 K. At temperatures higher than 4800 K it decomposes to H ions and O ions [21]. Thus, the water vapor decomposes to H ions and O ions entirely in the center of arc during welding process because the temperature of arc center is about 5000 K–50,000 K [22]. The solubility of H ions decreases sharply from 0.69 mL/100 g to 0.036 mL/100 g under equilibrium conditions. The amount of water vapor and the decomposition amount of water vapor increase with the increase of humidity. Then the amount H ions and the pressure of H vapor increases in the high temperature arc and probability of porosity formation increases and the quantity accumulates as a result.

From the result of Table 4 and Fig. 5, the porosity quantity under the 90% humidity is 2.8 times higher than that under the 70% humidity. The mean size of porosity under the 70% humidity is 12.5 times higher than that under the 90% humidity. The maximum diameter of porosity under the 70% humidity is 4.5 times higher than that under the 90% humidity. The total area of porosity under the 70% humidity is 4.6 times higher than that under the 90% humidity. The maximum area of porosity under the 70% humidity is 17.8 times higher than that under the 90% humidity. The porosity possession rate under the 70% humidity is 3.6 times higher than that under the 90% humidity. Thus, it can be concluded that the major factors that influence the properties of welded joints were porosity size and the possession rate. The distribution of maximum porosity affects the properties of weld joints. Hence, the 70% humidity is the critical level of humidity for welding.

4. Conclusion

The A7N01S-T5 welded joints were fabricated under different environment humidity using gas metal arc welding process in an environment simulation lab. The microstructures and porosity quantities were investigated using an optical microscope and analysis software. The fatigue properties were also measured for all humidity conditions. The following conclusions can be drawn:

- The microstructures of the weld and HAZ were similar under different environment humidity.
- The porosity quantity increased with the increase of humidity and the porosities under the 90% humidity condition had the maximum quantity. However, the porosity under the 70% humidity condition had the maximum mean size, maximum diameter, maximum area, maximum total area, maximum sectional total area, and maximum possession rate.
- The mean fatigue strength of welded joints decreased from the 50% humidity condition to the 70% humidity condition and then increased to the 90% humidity condition. The fracture mechanism of welded joints under the 70% humidity condition was brittle fracture, while others were ductile fracture.
- The major factors that affect the weld-joint properties were the porosity size and possession rate, especially the distribution of maximum porosity. The 70% humidity condition was the critical level for environment humidity during welding.

Acknowledgments

The results of this paper were from the projects, “Effect of Residual Stress on the Corrosion Behaviour in Weld Joints and Development of Control Technology for Car Bodies in Aluminum–Alloy Trains” and “Research of the Key Technologies And Equipment for Next-Generation Railway Transportation In Cities.” The authors acknowledge the financial support by the scientific and technological innovation projects of the Chinese Central Universities (No.2682014CX003) and the financial support by the National Science & Technology Pillar Program (No. 2015BAG12B01).

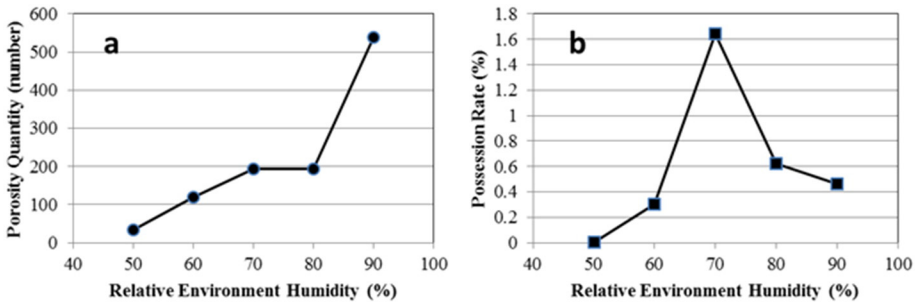

Fig. 5. Porosity quantity and possession rate as a function of relative humidity. (a) Porosity quantity; (b) possession rate.

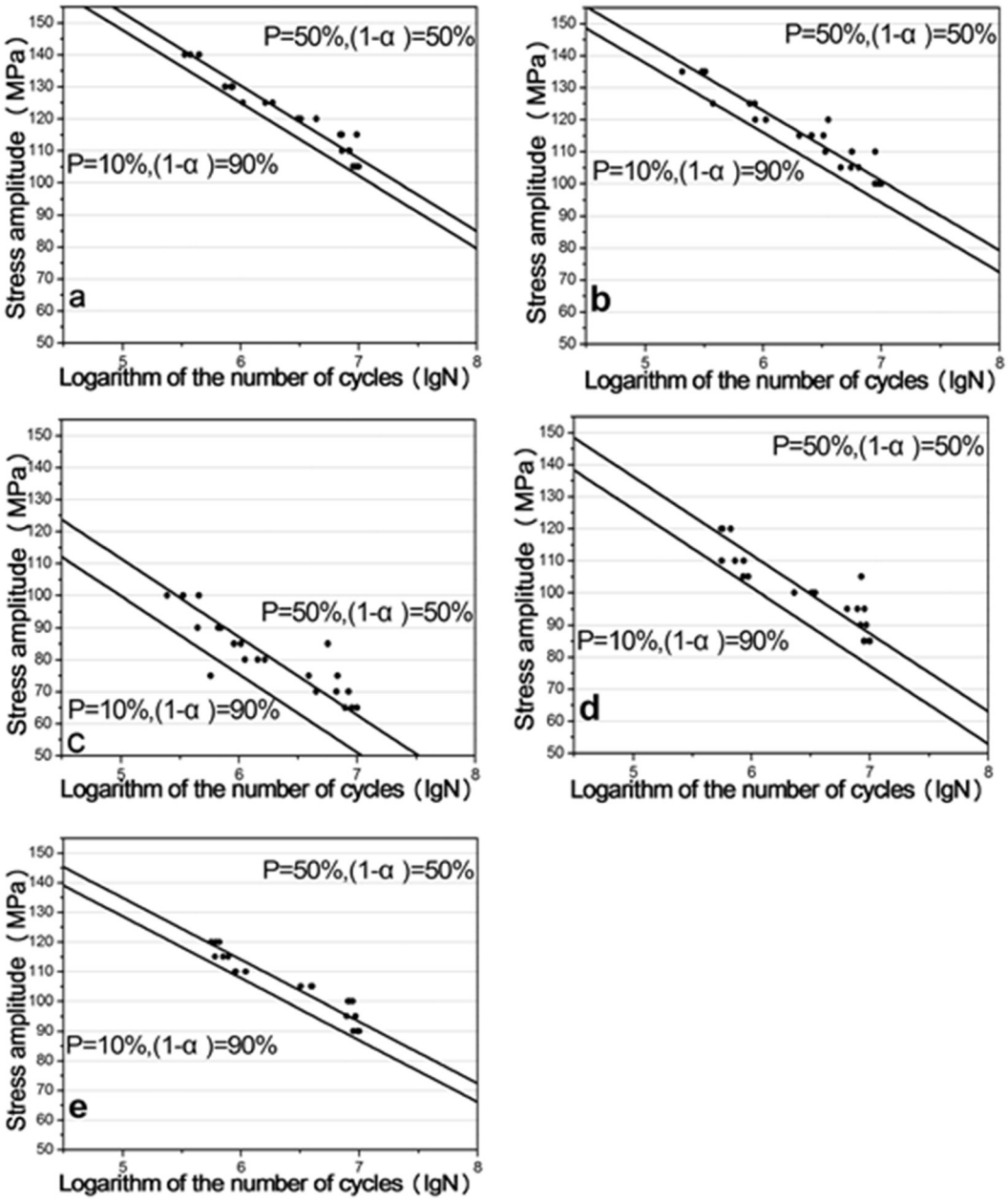

Fig. 6. P–S–N curves of welded joints under different humidity. (a) Under 50% humidity; (b) under 60% humidity; (c) under 70% humidity; (d) Under 80% humidity; (e) Under 90% humidity.

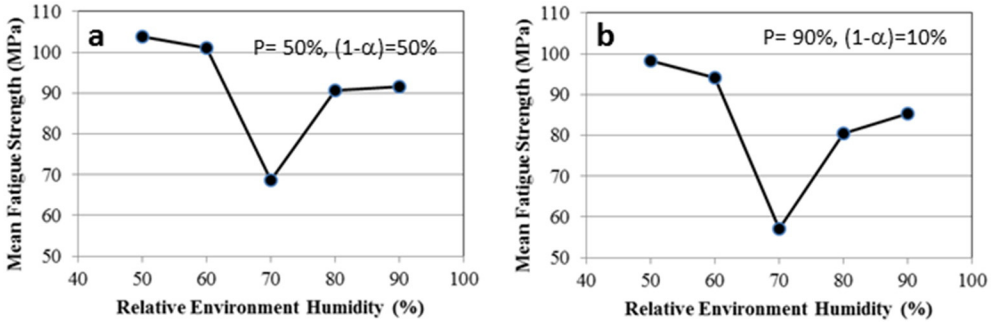

Fig. 7. Mean fatigue strength of welded joints under different humidity. (a)Under 50% failure probability (b) under 10% failure probability.

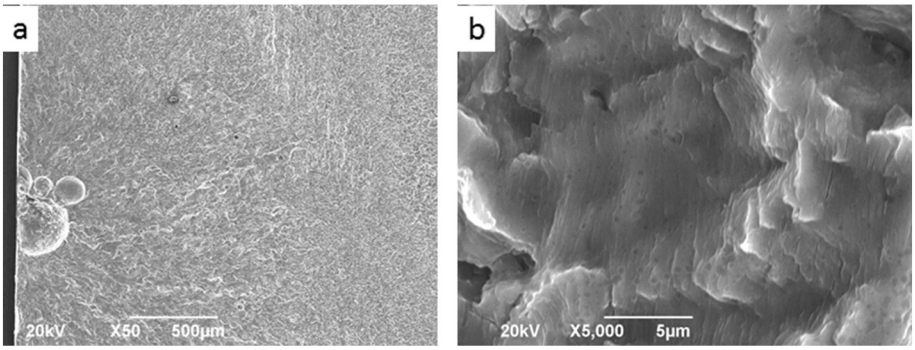

Fig. 8. Fracture morphologies of a fatigue sample under the 50% humidity. (a) Crack source zone; (b) crack propagation zone.

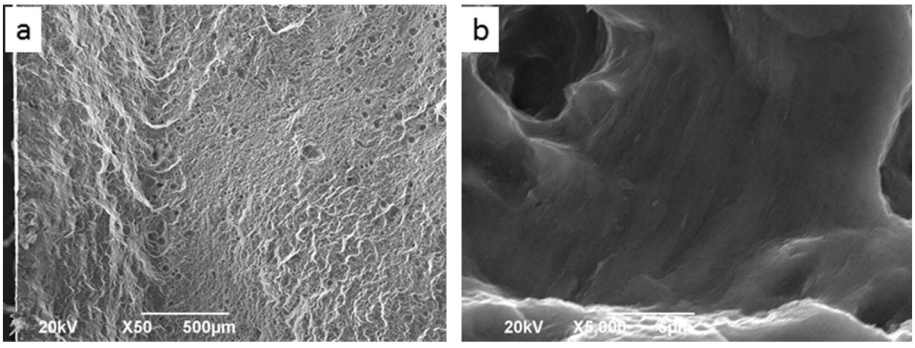

Fig. 9. Fracture morphologies of welded joints under 60% humidity. (a) Crack source zone; (b) crack propagation zone.

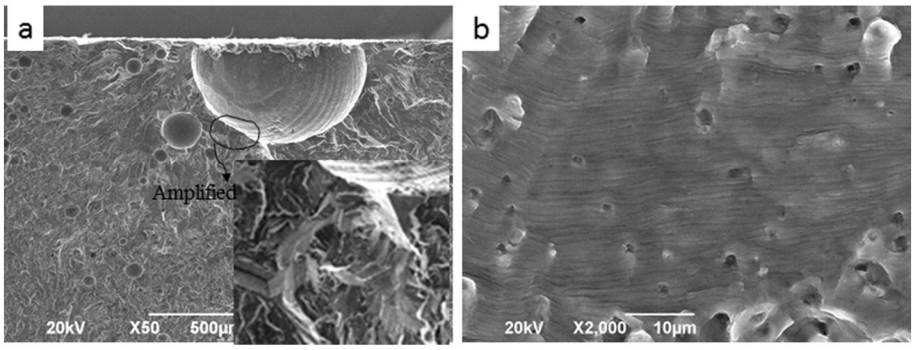

Fig. 10. Fracture morphologies of welded joints under 70% humidity. (a) Crack source zone; (b) crack propagation zone.

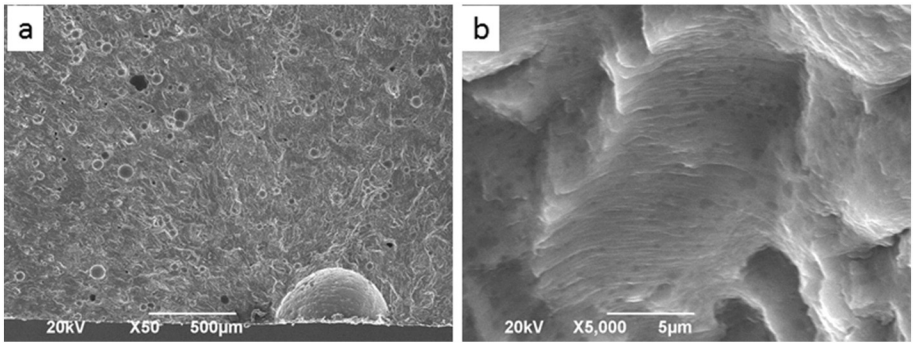

Fig. 11. Fracture morphologies of welded joints under 80% humidity. (a) Crack source zone; (b) crack propagation zone.

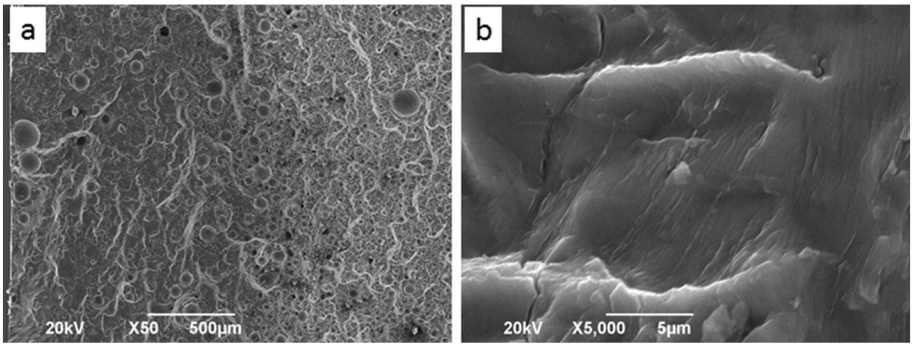

Fig. 12. Fracture morphologies of welded joints of 90% humidity. (a) Crack source zone; (b) crack propagation zone.

References

[1] Y. Zhou, J. Liu, Q. Wang, M. Zhang, H. Chen, Failure analysis of A7N01S-T5 aluminum alloy buffer beam for high-speed train, Adv. Mater. Res. 652–654 (2013) 1290-1294.
[2] X. Zhang, C. Ma, G. Gou, Y. Liu, H. Chen, H. Li, Failure analysis of A7N01S-T5 aluminum alloy crossbeam for high speed train, Corros. Prot. 34 (3) (2013) 258–261.
[3] X. Wang, X. Liao, C. Ma, S. Zhang, Y. Liu, H. Chen, Effects of chemical composition on the corrosion behavior of A7N01S-T5 Al alloys, Int. J. Mod. Phys. B 29 (10) (2015)http://dx.doi.org/10.1142/S0217979215400251.
[4] H. Yua, Y. Xub, J. Songa, J. Pua, X. Zhaoa, G. Yaoa, On-line monitor of hydrogen porosity based on arc spectral information in Al–Mg alloy pulsed gas tungsten arc welding, Opt. Laser Technol. 70 (2015) 30–38.
[5] J. Zhang, J. Shan, J. Ren, P. Wen, Reducing the porosity in die-cast, magnesium alloys during laser welding, Weld. J. 92 (4) (2013) 101s–109s.
[6] X.L. Gao, L.J. Zhang, J. Liu, J.X. Zhang, Porosity and microstructure in pulsed Nd:YAG laser welded Ti6Al4V sheet, J. Mater. Process. Technol. 214 (7) (2014) 1316–1325.
[7] M. Mazar Atabaki, J. Ma, W. Liu, R. Kovacevic, Pore formation and its mitigation during hybrid laser/arc welding of advanced high strength steel, Mater. Des. 67 (2015) 509–521.
[8] J. Li, M. Zhang, Y. Zhao, Z. Lin, Control of porosities in aluminum alloys welds and research of welding joint property, J. East China Shipbuilding Inst. (Nat. Sci. Ed.) 18 (5) (2004) 78–81.
[9] R.F. Ashton, R.P. Wesley, C.R. Dixon, The effect of porosity on 5086-H116 aluminum alloy welds, Weld. J. 54 (3) (1975) 95s–97s.
[10] H. Mayer, M. Papakyriacou, B. Zettl, S.E. Stanzl-Tschegg, Influence of porosity on the fatigue limit of die cast magnesium and aluminium alloys, Int. J. Fatigue 25 (2003) 245–256.
[11] Z. Zhou, Metal Welding Principles and Processes, Machinery Industry Press, Beijing, 1981.
[12] M. Wahba, M. Mizutani, Y. Kawahito, S. Katayama, Laser welding of die-cast AZ91D magnesium alloy, Mater. Des. 33 (1) (2012) 569–576.
[13] M. Harooni, B. Carlson, B.R. Strohmeier, R. Kovacevic, Pore formation mechanism and its mitigation in laser welding of AZ31B magnesium alloy in lap joint configuration, Mater. Des. 58 (2014) 265–276.
[14] A. Munitz, C. Cotler, A. Stern, G. Kohn, Mechanical properties and microstructure of gas tungsten arc welded magnesium AZ91D plates, Mater. Sci. Eng. A 302 (2001) 68–73.
[15] R. Zeng, J. Zhang, W. Huang, W. Dietzel, K.U. Kainer, Review of studies on corrosion of magnesium alloys, Trans. Nonferrous Metals Soc. China 16 (2006) 763–771.
[16] A. Melander, M. Larsson, H. Stensio, Fatigue performance of weldbonded high strength sheet steels tested in arctic, room temperature and tropical environments, Int. J. Adhes. Adhes. 20 (5) (2000) 415–420.
[17] C.F. Korenberg, A.J. Kinloch, J.F. Watts, Crack growth of structural adhesive joints in humid environments, J. Adhes. 80 (3) (2004) 169–201.
[18] X. Zhou, Y. Lu, Z. Fu, Y. Gong, Effect of temperature and humidity in environment on porosity formation in welding LD10 aluminium alloy, Proceedings of International Conference on Quality and Reliability in Welding, 5 1984, pp. 1–6.
[19] R.J. Shore, R.B. McCauley, Effects of porosity on high strength aluminum 7039, Weld. J. 49 (7) (1970) 311s–321s.
[20] J.F. Rudy, E.J. Rupert, Effects of porosity on mechanical properties of aluminum welds, Weld. J. 49 (7) (1970) 322s–336s.
[21] X. Fu, Physics Chemistry, High Education Press, Beijing, 2005.
[22] S. Huang, Arc Welding Power and Digital Control, Machinery Industry Press, Beijing, 2010.